

Itinerant spin density waves in repulsively interacting spin-orbit coupled Fermi gas

Shang-Shun Zhang^{1,2}, Jinwu Ye^{2,3}, and Wu-Ming Liu¹

¹*Beijing National Laboratory for Condensed Matter Physics,*

Institute of Physics, Chinese Academy of Sciences, Beijing 100190, China

²*Department of Physics and Astronomy, Mississippi State University, MS 39762, USA*

³*Key Laboratory of Terahertz Optoelectronics, Ministry of Education,
Department of Physics, Capital Normal University, Beijing 100048, China*

(Dated: December 3, 2024)

We investigate the magnetic orderings of repulsively interacting Fermi gases with a Weyl spin-orbit coupling (SOC). We classify the symmetries the SOC Hamiltonian and find their exact constraints on the density-spin response functions. We show that a putative ferromagnetic (FM) state is always unstable against a transverse spin density wave (SDW) state. The SOC provides a new and efficient mechanism to realize various SDW at relatively weak repulsive interactions. In the para-magnet (PM) side, we identify one gapless sound mode and three gapped modes (one longitudinal and two transverse modes). The SOC leads to the splitting of two transverse modes at any finite momentum. As the interaction increases, the PM turns into the stripe Transverse-SDW or Longitudinal-SDW at small or large SOC strengths respectively whose pitch is determined by the SOC strength. There is an accompanying CDW to the LSDW with twice its pitch. There are different collective excitations and FS re-constructions inside the TSDW and LSDW+CDW. We construct quantum bosonic Lifshitz actions to study the transitions from PM to TSDW or LSDW+CDW. Various experimental probes of these novel phenomena are discussed. Implications and connections to stripe ordered states in various condensed matter systems are made.

PACS numbers: 03.75.Ss, 05.10.Cc, 68.35.Rh, 67.80.dk

Introduction— The investigation and control of spin-orbit (SO) coupling have become subjects of intensive research in condensed matter and cold atoms since the discovery of the topological insulators [1, 2]. It was found to be a critical factor leading to a whole new class of electronic states in *correlated* electron materials [3]. In cold atom systems, the recent experimental realizations of 1d SOC [4, 5] and the proposals to realize the 2d Rashba or Dresselhaus SOC [6] and 3d isotropic (Weyl) SOC [7] for neutral cold atoms inspired extensive theoretical investigations on various important effects of SOC on the pairing physics of attractively interacting Fermi gases [8, 9]. However, there are still relatively few works in the repulsive side which could provide a new paradigm to realize different spin and orbital symmetry breaking states [10–14].

On the other front, studying competing orders among paramagnet (PM), ferromagnetism (FM), spin density waves (SDW) and charge density waves (CDW) in itinerant fermionic systems is a long-standing goal in material science. It dates back to the Stoner’s instability [15–17] and upto recent doping dependent stripe charge and spin orderings in high temperature superconductors [18, 19]. In cold atom systems, there were both experimental [20] and theoretical work [21] on possible FM in a purely repulsively interacting two component Fermi systems. But so far, possible dramatic effects of SOC on the competing orders in the fermionic systems have not been discussed.

In this Letter, we study the competing orders in a repulsively interacting Fermi gas with a 3d Weyl SOC. We find the SOC leads to dramatic differences than in Fermi

gas without it. We present a systematic symmetry classifications of the SOC Hamiltonian and establish their exact constraints on various density-spin correlation functions. In the PM, we identify one gapless sound mode and three gapped modes. The Weyl SOC leads to the splitting of two transverse modes at any finite momentum, which indicates a possible stripe transverse SDW order. From the exact constraints, we show that a putative FM is always unstable against a possible TSDW. Indeed, as interaction increases, the PM becomes a stripe transverse (chiral, spiral and co-planar) SDW at small or intermediate SOC and a stripe longitudinal (collinear) SDW at large SOC. The stripe ordering wavevector Q_T of the TSDW and Q_L of the LSDW are continuously tuned by the SOC strength. There is an accompanying stripe CDW order to the LSDW with $Q_C = 2Q_L$. The critical interaction strengths are dramatically reduced due to the nearly flat band structure near the bottom (Weyl shell) of the spectrum. The collective excitations in the two states are also studied. There are also corresponding Fermi Surface (FS) reconstructions inside the TSDW and LSDW+CDW. The spin flop transition from the TSDW to the LSDW+CDW is a first order transition. We also construct quantum bosonic Lifshitz actions to study the PM to TSDW or LSDW+CDW transition. In view of the rapid technical developments of cold atoms in Bragg spectroscopy [23, 24], speckling, tomographic, specific heat and *In-Situ* measurements [25–29], our theoretical predictions could be probed in near future experiments in both cold atoms and relevant condensed matter systems.

Path Integral formulation.—We consider a repulsively

interacting two-component Fermi gas with the isotropic Weyl SOC $V_{SO} = \lambda \vec{k} \cdot \vec{\sigma}$, described by the Hamiltonian

$$H = \int d^3 \vec{r} [\Psi^\dagger \left(\frac{-\hbar^2 \nabla^2}{2m} - \mu + V_{SO} \right) \Psi + g \int d^3 \vec{r} \Psi_\uparrow^\dagger(\vec{r}) \Psi_\downarrow^\dagger(\vec{r}) \Psi_\downarrow(\vec{r}) \Psi_\uparrow(\vec{r})], \quad (1)$$

where the SOC strength $\lambda = \frac{g_F \mu_B \nabla B}{3m\hbar}$ can be tuned by the magnetic field gradient ∇B in the scheme [6, 7], g_F the Landé factor and μ_B the Bohr magneton, $g = 4\pi\hbar^2 a_s/m$ with a_s the s -wave scattering length. The chemical potential μ is determined by the density of atoms self-consistently. Because in cold atom experiments, the density is fixed, so it is convenient to take $k_R = m\lambda$ as the momentum unit and $E_R = k_R^2/2m$ as the energy unit. We characterize the SOC strength by the dimensionless ratio $\gamma = k_R/k_F$ where $k_F = (6\pi^2 n)^{1/3}$ is the Fermi momentum of the system without SOC at the same density n . we set $\hbar = k_B = 1$.

The interaction can be divided into the density and spin channel $\mathcal{H}_I = \frac{g}{8} \int d\vec{r} [\rho(\vec{r})^2 - \vec{S}(\vec{r})^2]$, where $\rho(\vec{r}) = \Psi^\dagger \Psi(\vec{r})$ and $\vec{S}(\vec{r}) = \Psi^\dagger \vec{\sigma} \Psi(\vec{r})$. In the presence of SOC, the density fluctuation is coupled with the spin fluctuation[11]. We introduce the density-spin order parameter $\phi_\mu, \mu = n, x, y, z$ to decouple the interaction term via a Hubbard-Stratonovich transformation. Integrating out the fermionic fields leads to the effective action for ϕ_μ :

$$S = \int d^3 \vec{r} \int_0^{1/T} d\tau \frac{1}{2g} \phi_\mu^2 - \text{Tr} \ln (-\mathcal{G}_0^{-1} + M), \quad (2)$$

where $\mathcal{G}_0^{-1} = -\partial_\tau - \mathcal{H}_0 + \mu$, $M = \frac{i}{2} \phi_n \sigma^0 + \frac{1}{2} \vec{\phi} \cdot \vec{\sigma}$.

The density channel ϕ_n has a non-zero imaginary saddle point value due to the finite particle density of the fermions which could be eliminated by re-defining $\delta\phi_n$ as the deviation from its saddle point value. To the second order of $\delta\phi_\mu$, we obtain: $\mathcal{S}_H^{(2)} = 1/(2\beta V) \sum_{\vec{q}, n} \mathcal{K}^{\mu\nu} \delta\phi_\mu(-\vec{q}, -i\omega_n) \delta\phi_\nu(\vec{q}, i\omega_n)$, where $\mathcal{K}^{\mu\nu} = \delta^{\mu\nu}/g - \bar{\chi}^{\mu\nu}(\vec{q}, i\omega_n)/4$, $\bar{\chi}^{\mu\nu}$ is related to the usual density-spin susceptibility $\chi^{\mu\nu}(\vec{q}, i\omega_n) = \langle s^\mu(\vec{q}, i\omega_n) s^\nu(-\vec{q}, -i\omega_n) \rangle$ via $\bar{\chi}^{00} = -\chi^{00}$, $\bar{\chi}^{0i} = i\chi^{0i}$, $\bar{\chi}^{ij} = \chi^{ij}$ with $i, j = x, y, z$.

Symmetry analysis of the SOC Hamiltonian.— Before performing any analytical or numerical calculations, it is important to investigate the symmetries of the systems and their implications on experimentally observable physical quantities. The symmetry analysis for interacting SOC systems are very different from any previously known (non)-relativistic systems and have never been systematically discussed before [9, 13]. Here, we classify the symmetries of the 3d Weyl SOC Hamiltonian Eqn.1 and also find their exact constraints on various density-spin correlation functions. In Sec.VI, we will present the symmetry breaking patterns of the itinerant

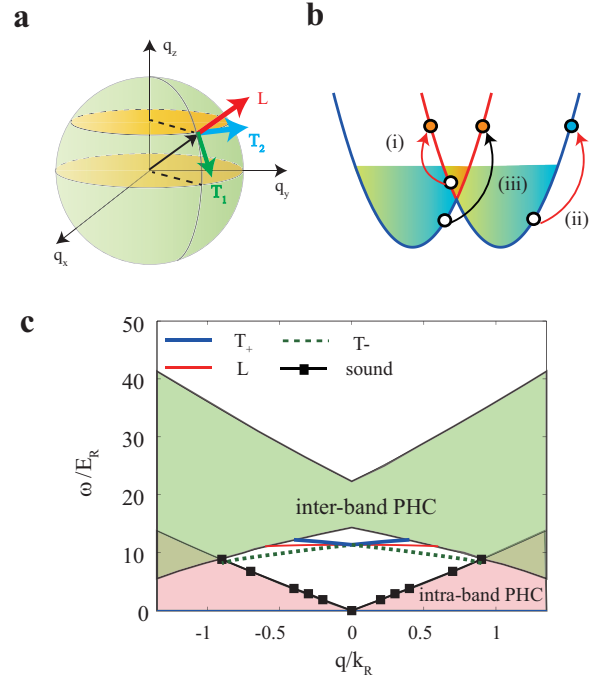


FIG. 1. (Color online) (a) The helicity basis shows one longitudinal mode and two transverse modes. (b) The schematic plot of the intra-band (process (i) and (ii)) and inter-band (process (iii)) particle-hole excitations. (c) The collective modes in the normal state at $\gamma = 0.58$. The pink (green) regime represents the intra-(inter) band particle-hole excitation as shown in (b). The split T_{\pm} modes indicate possible TSDW at $\vec{q} = \pm Q_T \hat{z}$.

FM and the counting of the collective excitations above the FM phase.

For the Weyl SOC, the symmetries of the Hamiltonian Eqn.1 are: (i) Continuous $[SU(2)_{spin} \times SO(3)_{orbit}]_D$, where the subscript D represents the simultaneous rotations in both spin and orbital space. (ii) the time reversal symmetry \mathcal{T} : $\mathcal{T} \Psi_{\vec{k}\uparrow} \mathcal{T}^{-1} = \Psi_{-\vec{k}\downarrow}$ and $\mathcal{T} \Psi_{\vec{k}\downarrow} \mathcal{T}^{-1} = -\Psi_{-\vec{k}\uparrow}$ which imply $\vec{S} \rightarrow -\vec{S}, \vec{k} \rightarrow -\vec{k}, i \rightarrow -i$. (iii) Three spin-orbital coupled discrete symmetries: $\mathcal{P}_x = [\mathcal{I}_x \times \mathcal{S}_x]_D$ where $\mathcal{I}_x : p_x \rightarrow p_x, p_{y,z} \rightarrow -p_{y,z}$ the spatial reflection operator about x axes and $\mathcal{S}_x : s_x \rightarrow s_x, s_{y,z} \rightarrow -s_{y,z}$ a π rotation about S_x axes; Similarly, there are other two discrete symmetries: $\mathcal{P}_y = [\mathcal{I}_y \times \mathcal{S}_y]_D$ and $\mathcal{P}_z = [\mathcal{I}_z \times \mathcal{S}_z]_D$. Note that the \mathcal{P}_z is just a special case of $[SU(2)_{spin} \times SO(3)_{orbit}]_D$ symmetry with a π rotation about S_z axes. These symmetries can be used to establish exact relations on the spin-density correlation functions some of which are listed here, the details are given in the SM.

In the presence of SOC, it is convenient to define a helical basis (Fig. 2 (a)) where we can define two transverse spin modes ($\hat{T}_1 \cdot \vec{S}, \hat{T}_2 \cdot \vec{S}$) and one longitudinal L spin mode ($\hat{q} \cdot \vec{S}$). The $[SU(2)_{spin} \times SO(3)_{orbit}]_D$ symme-

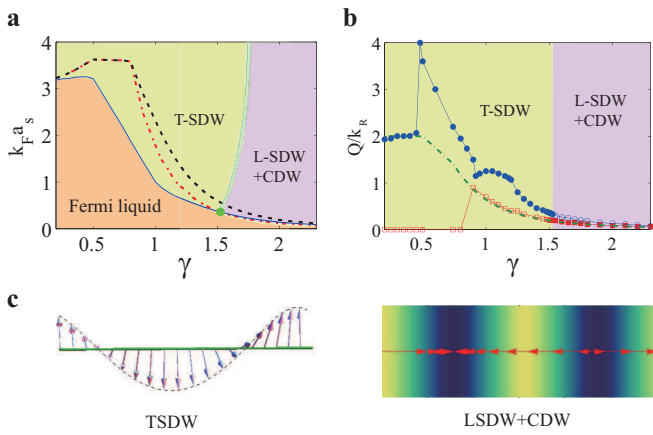


FIG. 2. (Color online) (a) The critical interaction strength from the PM to TSDW (blue line), LSDW+CDW (red dashed dotted line) or a putative FM (black dashed line) transition. The FM is always unstable against the TSDW, in sharp contrast to a 3d Fermi system without SOC (See SM). The transition from the PM to TSDW or LSDW+CDW is of the bosonic Lifshitz type, that from TSDW to LSDW+CDW is first order. (b) The ordering wavevector Q_T (blue circles) and Q_L (red squares) of the TSDW and LSDW as a function of SOC strength γ . The green dot-dashed line represents the $k_{F_2} - k_{F_1}$. When $\gamma < 0.5$, $Q_T \sim k_{F_2} - k_{F_1}$ is dominated by the momentum transfer between outer FS and inner FS with the opposite helicity, When $0.5 < \gamma < 1.5$, Q_T is dominated by other momentum transfer processes. When $\gamma > 1.5$, $Q_L \sim k_{F_2} - k_{F_1}$ is dominated by the momentum transfer between outer FS and inner FS with the same helicity. (c) Schematic plot of the TSDW and LSDW+CDW orders.

try dictates that the dynamic 4×4 density-spin response function $\chi^{\mu\nu}(\vec{q}, \omega)$ can be split into two 2×2 subspaces: i) $n - L$ subspace ii) $T_1 - T_2$ subspace.

In the $T_1 - T_2$ subspace, after a unitary transformation, it can be shown that

$$\chi = \begin{pmatrix} \chi^{+-} & 0 \\ 0 & \chi^{-+} \end{pmatrix}, \quad \chi^{+-}(\vec{q}, \omega) = \chi^{-+}(-\vec{q}, \omega) \quad (3)$$

whose poles lead to two gapped transverse collective modes T^+, T^- respectively.

In the $n - L$ subspace,

$$\begin{aligned} \chi^{nn}(\vec{q}, \omega) &= \chi^{nn}(-\vec{q}, \omega), \quad \chi^{LL}(\vec{q}, \omega) = \chi^{LL}(-\vec{q}, \omega) \\ \chi^{nL}(\vec{q}, \omega) &= \chi^{Ln}(\vec{q}, \omega) = -\chi^{nL}(-\vec{q}, \omega), \end{aligned} \quad (4)$$

Diagonalization in the $n - L$ space leads to a gapless sound mode and a gapped L mode.

These exact relations can be used to simplify considerably the following analytical and numerical calculations to find the 4 collective modes and also the form of effective actions inside the P-H continuum. Any approximations such as RPA calculations in the following sections should respect these exact relations.

Collective modes in the PM.— Adding density-spin

sources to Eq. (2) and integrating out $\delta\phi_\mu$, one can extract collective modes through the poles of density-spin response functions at the RPA level. We checked that they all satisfy the exact relations Eqn.3 and 4. In the $n - L$ subspace, the mixing of density and longitudinal mode leads to one gapless sound (black) mode $\omega_q^s = v_s q$ and one gapped (called L) (green) mode $\omega_L(\vec{q}) = \Delta + \alpha q^2$ where $\alpha < 0$ (Fig.1c). In the $T_1 - T_2$ subspace, there are two split transverse modes $\omega_{T_{+/-}}(\vec{q}) = \Delta \pm \beta q_z$ (Fig.1c). The T_+ mode (red) is the pole of χ^{+-} , while T_- (blue) is the pole of χ^{-+} . As shown in the SM, the split of the two transverse modes for finite q are due to the absence of inversion symmetry (or equivalently \mathcal{S}_x or \mathcal{S}_y symmetry) of the Weyl SOC. The exact symmetry Eqn.3 indicates T_+ and T_- exchanges under $q_z \rightarrow -q_z$. The restored $SU(2)_{spin}$ symmetry at $\vec{q} = 0$ dictates that the three gapped modes must have the same gap Δ at $q = 0$. We find Δ vanishes for interaction strength larger than $g_s = 24\pi^2 k_R / m(k_{F_2}^2 - k_{F_1}^2)$, where $k_{F_2} > k_{F_1}$ are the two Fermi momenta in the presence of SOC. This corresponds to an instability driven by the collective modes at $q = 0$.

Fig.1c shows that $\omega_{T_{+/-}}(\vec{q}) = \Delta \pm \beta q_z$ may become negative simultaneously at $\pm Q_T \hat{z}$ before $\Delta = 0$ at $q = 0$. This indicates a transverse (spiral, chiral and co-planar) SDW transition at $\pm Q_T \hat{z}$ with the order parameter $\vec{\phi}_T = \phi_0(\cos Qz, \sin Qz, 0)$. In the following, we will study such an instability in the P-H channel.

Absence of FM instability.— There is also a FM instability when the static spin susceptibility diverges at $\delta = \frac{1}{g_c} - \frac{\chi_0}{4} = 0$, i.e., the Stoner FM instability. Here $\chi_0(\vec{q} \rightarrow 0, \omega = 0) = \frac{m}{6\pi^2} \left(\frac{k_{F_1}^2 + k_{F_2}^2}{K} + \frac{k_{F_2}^2 - k_{F_1}^2}{k_R} \right)$, $K = \sqrt{k_R^2 + 2m\mu}$ is the static spin susceptibility of 3D non-interacting Fermi gas with the Weyl SOC. We obtain the critical value of dimensionless interaction strength $k_F a_s^c = F(\gamma)$ as shown in Fig.2a. As γ increases, $F(\gamma)$ has a maximum at $\gamma \simeq 0.63$ corresponding to the chemical potential $\mu = -\frac{2}{3}E_R$, after which, $k_F a_s^c$ decreases quickly. At a strong SOC, the μ approaches the bottom of the spectrum (the Weyl shell at $|\vec{k}| = k_R$) where the density of states diverges as $\frac{1}{\sqrt{\epsilon}}$. The effects of an interaction are dramatically enhanced, even a weak interaction may drive the system into the itinerant FM state.

Because $g_c < g_s$, the FM instability happens before that driven by the $q = 0$ instability of the collective modes. However, to find out if it happens before the possible TSDW instability at $\pm Q_T \hat{z}$ mentioned above, it is tempting to construct a quantum Ginzburg-Landau action to describe the putative paramagnet-FM transition. Taking the $\vec{q} \rightarrow 0, \omega/v_F q \rightarrow 0$ limit and integrating out the non-critical density mode, one obtains the effective action in terms of the spin fluctuation order parameters

consistent with all the symmetries of the Hamiltonian:

$$\mathcal{S} = \int \frac{d^3 \vec{q}}{(2\pi)^3} T \sum_n \frac{1}{2} \mathcal{G}_s^{-1} \hat{P}_s^{ij} \phi_i \phi_j + u \int d^3 \vec{r} d\tau (\vec{\phi}^2)^2, \quad (5)$$

where $\hat{P}_s^{ij} = \hat{n}_s^i \hat{n}_s^j$ ($\hat{n}_s = \hat{T}_+, \hat{T}_-, \hat{L}$) is the projection operator into the helical basis, $\mathcal{G}_{T_\pm}^{-1} = \delta + \gamma_T |y| \pm \beta_T q + \alpha_T q^2$ and $\mathcal{G}_L^{-1} = \delta + \gamma_L y^2 + \alpha_L q^2$ where $y = \omega_n / v_F q$ are the propagators of the helical spin modes. We observe that the $\pm q$ terms in the transverse propagators are dictated by the exact symmetry Eqn.3. They indicate that the putative FM is always unstable to a TSDW at a finite q determined by the divergence of the static transverse susceptibility $\chi^{+-}(Q_T, \omega = 0)$ [22]. Extensive numerical calculations on the collective modes inside the putative FM also find that they become negative in some momentum regimes, indicating the instability of the putative FM state.

TSDW at $\gamma < 1.5$.— The instabilities in both the collective mode and the P-H channel dictated by the exact symmetry Eqn.3 point to the formation of the TSDW before the FM. Here we search for the pole of $\chi^{+-}(Q_T \hat{z}, \omega = 0)$ of the T_+ mode. Due to the exact relation Eqn.3, one also gets the pole at $\chi^{-+}(-Q_T \hat{z}, \omega = 0)$ due to the T_- mode. So $\pm Q_T$ has to appear in pair, indicating $\langle S_+ \rangle = e^{i(Q_T z + \theta)}$, $\langle S_- \rangle = e^{-i(Q_T z + \theta)}$ which is a chiral (also spiral) SDW. The critical interaction strength $k_F a_s$ and the orbital momentum Q_T are shown in Fig.2a and 2b respectively. The symmetry breaking from the paramagnet to the TSDW is $[SU(2)_{spin} \times SO(3)_{orbit}]_D \times Tran \rightarrow [U(1)_{spin}^z \times U(1)_{orbit}]_D \times (z \rightarrow z + \alpha/Q_T)$. Of course, when $\alpha = 2\pi$, it reduces to just a translation by a lattice constant $z \rightarrow z + a$. This symmetry breaking leads to one gapless Goldstone mode θ in $\vec{\phi}_T = \phi_0(\cos(Qz + \theta), \sin(Qz + \theta), 0)$. It is a coupled lattice phonon and transverse spin mode and can be considered as the remnant of the T_\pm modes in Fig.1a. By a symmetry analysis, we get the effective action of the mixed mode $\mathcal{L}_T[\theta] = (\partial_\tau \theta)^2 + a_T (\partial_z \theta)^2 + b_T (\partial_\perp \theta)^2$. There is a finite temperature 3d XY transition driven by the vortex un-binding in the phase of the mixed Goldstone mode θ where the TSDW also melts. There is also a coupling between this mixed mode and the fermions with the FS shown in Fig.3a.

One can construct an effective action to describe the itinerant PM to the TSDW transition. After integrating out the massive ϕ_L mode and the density mode, we find the effective action takes a similar form as Eqn.5 where $\vec{\phi} = (\phi_1, \phi_2)$ and the transverse propagator is: $\mathcal{G}_{T_\pm}^{-1} = \delta_T + \gamma_T |\omega_n| + \alpha_T (q^2 - Q_T^2)^2$ with the dynamic exponent $z_T = 2$. When $\delta_T > 0$, it is in the PM state where $\langle \phi_+ \rangle = 0$. When $\delta_T < 0$, it is in the stripe TSDW state where $\langle \phi_+ \rangle = \phi_0 e^{i(Q_T z + \theta)}$. This is a bosonic Lifshitz transition which exists in various condensed matter systems such as the superfluid ^4He [30], exciton superfluids in bilayer quantum Hall or electron-hole bilayer [31]

and superconductor in a Zeeman field [32, 33]. It is a first order one leading to the stripe [32] TSDW.

LSDW+CDW at $\gamma > 1.5$.— The Fig.2a shows that when approaching to the bottom of the Weyl shell $\gamma > 1.5$, the TSDW turns into the LSDW $\vec{\phi}_L = \phi_0(0, 0, \cos(Q_L z + \theta))$ with the longitudinal ordering wavevector $Q_L \sim k_{F2} - k_{F1}$ (Fig.2b). There is also an accompanying CDW order with the charge ordering wavevector $Q_C = 2Q_L$: $\delta\phi_n = \phi_0^2 \cos(2Q_L z + 2\theta)$. The symmetry breaking from the PM to the LSDW + CDW is $[SU(2)_{spin} \times SO(3)_{orbit}]_D \times Tran \rightarrow [U(1)_{spin}^z \times U(1)_{orbit}]_D \times (z \rightarrow z + 2\pi/Q_L)$. It has one gapless lattice phonon mode θ , which maybe considered as the remnant of the L mode in Fig.1c. Note that at the static limit $\omega = 0$, $\chi_{ij}(\vec{q}, 0)$ in Eqn.4 is real, so $\chi_{nL}(\vec{q}, 0) = 0$, there is no coupling between the density and longitudinal mode at the quadratic level. We also find $\chi_{nn}(Q_L, 0)$ is finite, so the transition is *not* charge driven, in sharp contrast to the stripe charge ordering found in high T_c superconductors [18]. Following the classical GL action at $\omega = 0$ constructed in [18], we can see that the CDW is driven by the spin-ordering due to the cubic coupling $\lambda_3 \delta\phi_n \phi_L^2$. As shown in Fig.2a, at $\gamma \sim 1.5$, $Q_T > Q_L$, so the spin flop transition from LSDW + CDW to TSDW is first order.

As said above, the transition from the PM to the itinerant LSDW+CDW is spin driven, so after substituting the parasitic CDW order [18] and integrating out the two massive transverse modes T_\pm , we find the effective action takes a similar form as Eqn.5 where $\vec{\phi} = \phi_L$ and the longitudinal propagator is: $\mathcal{G}_L^{-1} = \delta_L + \gamma_L |\omega_n| + \alpha_L (q^2 - Q_L^2)^2$ with the dynamic exponent $z_L = 2$. When $\delta_L > 0$, it is in the PM state where $\langle \phi_L \rangle = 0$. When $\delta_L < 0$, it is in the stripe LSDW state where $\langle \phi_L \rangle = \phi_0 \cos(Q_L z + \theta)$. There is also an accompanying CDW. This is also a bosonic Lifshitz type of transition [30–32]. By symmetry analysis and drawing the analogy from the smectic liquid crystal [34], we get the effective action of the lattice phonon mode $\mathcal{L}_L[\theta] = (\partial_\tau \theta)^2 + a_L (\partial_z \theta)^2 + b_L (\partial_\perp \theta)^4$. At any finite temperatures, it becomes an algebraic ordered spin nematic state. There is also a coupling between this lattice phonon mode and the fermions with the FS shown in Fig.3b.

In the $\gamma \rightarrow \infty$ limit, or equivalently zero density limit, the system may become a Wigner crystal. In this limit, our RPA approach, which in principle, works for high density limit only, breaks down. A different approach such as a scaling argument treating the interaction non-perturbatively may be needed to work out the true ground state in such a zero density limit.

Fermi surface re-constructions in the TSDW and LSDW+CDW.— From Eqn.2, if ignoring the mixed Goldstone mode, one can see that the static TSDW $\langle \vec{\phi}_T \rangle = \phi_0(\cos(Q_T z, \sin Q_T z, 0)$ provides a periodic potential with a reciprocal lattice vector $Q_T \hat{z}$ to the fermions. Fig.3a shows the evolution of the FS as the

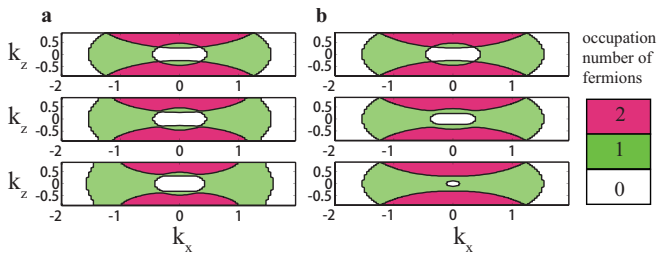


FIG. 3. (Color online) The Fermi surface at $\gamma = 0.8238$ and $Q = 1.8$ inside (a) the TSDW and (b) LSDW+CDW [35]. From up to down, the order parameter is increasing as $\phi = 0, 1, 2$. The fermion occupation number in the red, yellow, white regime are 2,1,0 respectively. The intersection of FS at the BZ boundary split inside the TSDW, but preserved inside the LSDW+CDW. The intersections between large and small FS inside the BZ boundary split in both phases. There is a rotation symmetry about the k_z axis.

TSDW turns on near the PM to TSDW transition. There is a gap Δ_{BZ}^T opening at the BZ boundary. First order degenerate perturbation shows that $\Delta_{BZ}^T = \phi_0 \cos^2 \frac{\theta}{2}$ where the θ is the polar angle of the crossing point between the FS and the 1st BZ boundary. There is also a gap Δ_I^T opening at the crossing between the outer FS and the inner FS inside the BZ, which is a new feature due to the SOC. First order degenerate perturbation shows that $\Delta_I^T = \phi_0 |\cos \frac{\theta_1}{2} \cos \frac{\theta_2}{2}|$ where the $\theta_{1,2}$ are the two polar angles of the two crossing FS momenta $\vec{k}_{F2} - \vec{k}_{F1} = Q_T \hat{z}$.

From Eqn.2, if ignoring the lattice phonon mode, one can see that the static LSDW $\langle \vec{\phi}_L \rangle = \phi_0(0, 0, \cos Qz)$ provides a periodic potential with a reciprocal lattice vector $Q_L \hat{z}$ to the fermions. Fig.3b shows the evolution of the FS as the LSDW turns on near the PM to LSDW transition. However, in sharp contrast to the TSDW, due the different symmetry breaking patterns in the LSDW+CDW, there is no gap opening at the BZ boundary $\Delta_{BZ}^L = 0$ which is consistent with the numerical calculations. However, there is still a gap Δ_I^L opening at the crossing between the outer FS and the inner FS inside the BZ, which is a new feature due to the SOC. First order degenerate perturbation shows that $\Delta_I^L = \phi_0 |\sin \frac{(\theta_1 - \theta_2)}{2}|$ where $\vec{k}_{F2} - \vec{k}_{F1} = Q_L \hat{z}$. FS reconstructions at other SOC strengths can be similarly mapped out. Similar gap opening at $Q_c = 2Q_L$ due to the CDW can be similarly evaluated by degenerate perturbations and numerical calculations.

Discussions. — The repulsively interacting Fermi gases with a Weyl SOC provides a completely new system displaying many novel properties. Its Hamiltonian has a new class of spin-orbital coupled symmetries which lead to important physical consequences. By exact symmetry analysis, we establish exact relations on various density-spin correlation functions and also show that there is no FM phase in the 3d Weyl SOC system [22]. By using

detailed calculations at the RPA level, we found that the PM will become unstable against itinerant stripe TSDW and the LSDW with coexisting CDW at weak interactions in repulsively interacting Fermi gas with a Weyl SOC. This is in sharp contrast to a repulsively interacting Fermi gas without a SOC where the FM could be a competing state (See SM). Their orbital ordering wavevectors Q_T and Q_L are determined by the SOC strength, in sharp contrast to high T_c superconductors where they are determined by the doping away from the Mott insulating limit [18]. In a ${}^6\text{Li}$ system, the two hyperfine sublevels $|1/2, -1/2\rangle$ and $|1/2, 1/2\rangle$ can be chosen as two pseudo-spin $1/2$ states. With $N \sim 10^4$ ${}^6\text{Li}$ atoms inside an isotropic trap with a trap frequency $2\pi \times 10\text{Hz}$, and a typical magnetic field gradient strength $\nabla B = 0.09G/\mu\text{m}$ (within practical range [36]), we estimate $\gamma \sim 1.82$. It falls into the LSDW regime with the the orbital momentum is $Q_L \sim 0.13k_R$. The critical interaction strength $k_F a_c \sim 0.12$ is order of magnitude smaller than the value π (Fig.1c at $\gamma = 0$) for a possible FM at the same density without the SOC [16, 21]. So experiments could easily reach the very weak interaction limit to reach both TSDW and LSDW+CDW. The itinerant TSDW and LSDW + CDW may display the anomalous Hall effect [37] and will be investigated in a future publication. As soon as the Weyl SOC is implemented in cold atom experiments, all these novel phenomena can be detected by various established experimental techniques[25–29]. The results achieved should also have deep and wide implications in many condensed matter systems.

This work was supported by the NKBRFC under grants Nos. 2011CB921502, 2012CB821305, NSFC under grants Nos. 61227902, 61378017, 11434015, and SPRP-CAS under grants No. XDB01020300. J. Ye was supported by NSF-DMR-1161497, NSFC-11174210.

-
- [1] M. Z. Hasan and C. L. Kane, Rev. Mod. Phys. **82**, 3045 (2010).
 - [2] X. L. Qi and S. C. Zhang, Rev. Mod. Phys. **83**, 1057 (2011).
 - [3] For a review, see A. M. Turner and A. Vishwanath, arXiv:1301.0330.
 - [4] Y. J. Lin, K. Jiménez-García, and I. B. Spielman, Nature (London) **471**, 83 (2011); P. Wang, Z. Q. Yu, Z. Fu, J. Miao, L. Huang, S. Chai, H. Zhai, and J. Zhang, Phys. Rev. Lett. **109**, 095301 (2012); L. W. Cheuk, A. T. Sommer, Z. Hadzibabic, T. Yefsah, W. S. Bakr, and M. W. Zwierlein, Phys. Rev. Lett. **109**, 095302 (2012).
 - [5] For a review, see J. Dalibard, F. Gerbier, G. Juzeliūnas, and P. Öhberg, Rev. Mod. Phys. **83**, 1523 (2011).
 - [6] Z.-F. Xu, L. You, and M. Ueda, Phys. Rev. A **87**, 063634 (2013).
 - [7] B. M. Anderson, G. Juzeliūnas, V. M. Galitski, and I. B. Spielman, Phys. Rev. Lett. **108**, 235301 (2012).
 - [8] Z. Q. Yu and H. Zhai, Phys. Rev. Lett. **107**, 195305

- (2011); H. Hu, L. Jiang, X. -J. Liu, and H. Pu, Phys. Rev. Lett. **107**, 195304 (2011); C. Qu, Z. Zheng, M. Gong, Y. Xu, L. Mao, X. Zou, G. Guo, and C. Zhang, Nat. Commun. **4**, 2710 (2013); W. Zhang and W. Yi, Nat. Commun. **4**, 2711 (2013); J. P. Vyasankere and V. B. Shenoy, Phys. Rev. B **83**, 094515 (2011); J. P. Vyasankere, S. Zhang and V. B. Shenoy, Phys. Rev. B **84**, 014512 (2011); Qi Zhou and Xiaoling Cui, Phys. Rev. Lett. **110**, 140407.
- [9] Yu Yi-Xiang, Jinwu Ye and W.M. Liu, Phys. Rev. A **90**, 053603 (2014).
- [10] Y. Li and C. Wu, Phys. Rev. B **85**, 205126 (2012).
- [11] S. S. Zhang, X. L. Yu, J. Ye, and W. M. Liu, Phys. Rev. A **87**, 063623 (2013).
- [12] Fadi Sun, X. -L. Yu, J. Ye, H. Fan, W. M. Liu, Scientific Reports **3**, 2119 (2013).
- [13] Fadi Sun, Jinwu Ye and Wu-Ming Liu, arXiv:1408.3399.
- [14] Fadi Sun, Jinwu Ye and Wu-Ming Liu, arXiv:1502.05338.
- [15] E. Stoner, Philos. Mag. **15**, 1018 (1933).
- [16] J. A. Hertz, Phys. Rev. B **14**, 1165 (1976).
- [17] A. J. Millis, Phys. Rev. B **48**, 7183 (1993); U. Zülicke and A. J. Millis, Phys. Rev. B **51**, 8996 (1995).
- [18] O. Zachar, S. A. Kivelson and V. J. Emery, Phys. Rev. B **57**, 1422 (1998). For a review, see S. A. Kivelson, I. P. Bindloss, E. Fradkin, V. Oganesyan, J. M. Tranquada, A. Kapitulnik, and C. Howald, Rev. Mod. Phys. **75**, 1201 (2003).
- [19] Jinwu Ye, Nucl. Phys. B **805** (3) 418-440 (2008).
- [20] G. B. Jo, Y. R. Lee, J. H. Choi, C. A. Christensen, T. H. Kim, J. H. Thywissen, D. E. Pritchard, and W. Ketterle, Science **325**, 1521 (2009).
- [21] R. A. Duine and A. H. MacDonald, Phys. Rev. Lett. **95**, 230403 (2005); V. B. Shenoy and T.-L. Ho, Phys. Rev. Lett. **107**, 210401 (2011); D. Pekker, M. Babadi, R. Sensarma, N. Zinner, L. Pollet, M. W. Zwierlein, and E. Demler, Phys. Rev. Lett. **106**, 050402 (2011); S. Pilati, G. Bertainia, S. Giorgini, and M. Troyer, Phys. Rev. Lett. **105**, 030405 (2010); X. Cui and T.-L. Ho, Phys. Rev. Lett. **110**, 165302 (2013); Phys. Rev. A **89**, 023611 (2014).
- [22] In 2d Rashba or Dresselhaus SOC, due to different symmetries, one can not rule out the FM phase.
- [23] M. Kozuma *et al.*, Phys. Rev. Lett. **82**, 871 (1999); J. Stenger *et al.*, *ibid.* **82**, 4569 (1999); D. M. Stamper-Kurn *et al.*, *ibid.* **83**, 2876 (1999); J. Steinhauer, R. Ozeri, N. Katz, and N. Davidson, *ibid.* **88**, 120407 (2002); S. B. Papp *et al.*, *ibid.* **101**, 135301 (2008); P. T. Ernst *et al.*, Nature Phys. **6**, 56 (2010).
- [24] Jinwu Ye, *et. al*, Phys. Rev. A **83**, 051604 (R) (2011); Ann. Phys. **328** (2013), 103-138.
- [25] C. Sanner, E. J. Su, A. Keshet, W. Huang, J. Gillen, R. Gommers, and W. Ketterle, Phys. Rev. Lett. **106**, 010402 (2011).
- [26] C. Sanner, E. J. Su, W. Huang, A. Keshet, J. Gillen, and W. Ketterle, Phys. Rev. Lett. **108**, 240404 (2012).
- [27] Y. Shin, C. H. Schunck, A. Schirotzek, and W. Ketterle, Nature (London) **451**, 689 (2008).
- [28] N. Gemelke, X. Zhang, C. -L. Huang, and C. Chin, Nature (London) **460**, 995 (2009).
- [29] J. Kinast, *et.al*, Science **25**, 1296-1299 (2005); M. J. H. Ku, *et.al*, Science **335**, 563-567 (2012).
- [30] Jinwu Ye, Phys. Rev. Lett. **97**, 125302 (2006), Europhysics Letters, **82** (2008) 16001, J. Low Temp Phys. **160**(3), 71-111,(2010). Yu Chen, Jinwu Ye and Quang Shan Tian, J. Low Temp Phys. **169** (2012), 149-168.
- [31] Jinwu Ye and Longhua Jiang, Phys. Rev. Lett. **98**, 236802 (2007); Jinwu Ye, Phys. Rev. Lett. **97**, 236803 (2006); Annals of Physics, **323** (2008), 580-630, J. Low Temp Phys. **158**(5), 882-900 (2010).
- [32] Longhua Jiang and Jinwu Ye, Phys. Rev. B **76**, 184104 (2007).
- [33] Leo Radzihovsky, Phys. Rev. A **84**, 023611 (2011).
- [34] P. M. Chaikin and T. C. Lubensky principles of condensed matter physics(Cambridge university press,1995.)
- [35] As shown in Fig.2b, at $\gamma = 0.8238$, the system is in the TSDW phase. Here we draw the FS reconstruction in the LSDW+CDW phase for a comparison.
- [36] M. Trinker, S. Groth, S. Haslinger, S. Manz, T. Betz, S. Schneider, I. Bar-Joseph, T. Schumm, and J. Schmiedmayer, Appl. Phys. Lett. **92**, 254102 (2008).
- [37] J. Ye, Y. B. Kim, A. J. Millis, B. I. Shraiman, P. Majumdar, and Z. Tešanović, Phys. Rev. Lett. **83**, 3737 (1999).

Supplementary Material for “Itinerant spin density waves of repulsive spin-orbit coupled Fermi gas”

Shang-Shun Zhang^{1,2}, Jinwu Ye^{2,3}, and Wu-Ming Liu¹

¹Beijing National Laboratory for Condensed Matter Physics,

Institute of Physics, Chinese Academy of Sciences, Beijing 100190, China

² Department of Physics and Astronomy, Mississippi State University, MS 39762, USA

³ Key Laboratory of Terahertz Optoelectronics, Ministry of Education,
Department of Physics, Capital Normal University, Beijing 100048, China

(Dated: December 3, 2024)

In this Supplementary material, in section I, we will first classify the symmetries of the 3d Weyl SOC Hamiltonian Eqn.M1 and also find their exact constraints on various density-spin correlation functions. In Sec.II, we compute the collective modes through the poles of density-spin response functions at the RPA level in the paramagnet side and also check against the exact relations established in the Sec.I. For a constructive comparison, we also evaluate the collective modes inside the itinerant FM state of a conventional system without SOC. In Sec.III, we will present the symmetry breaking patterns of the itinerant TSDW and LSDW+CDW, make some exact statements on the FS structures and also calculate the gap openings by degenerate perturbation theory. We use M to stand for the figures and equations in the main text.

I. SYMMETRY ANALYSIS OF WEYL SOC HAMILTONIAN

In the presence of Weyl SOC, it is convenient to define a helical basis (Fig.M1a) with respect to the momentum where we can define two transverse spin modes ($\hat{T}_1 \cdot \vec{S}$, $\hat{T}_2 \cdot \vec{S}$) and one longitudinal L spin mode ($\hat{q} \cdot \vec{S}$). The Hamiltonian has the following symmetries.

1. $[SU(2)_{spin} \times SO(3)_{orbit}]_D$ symmetry and also translational symmetry
2. Time reversal symmetry T : $Tc_{\vec{k},\uparrow}T^{-1} = c_{-\vec{k},\downarrow}$, $Tc_{\vec{k},\downarrow}T^{-1} = -c_{-\vec{k},\uparrow}$.
3. Three Spin-orbital coupled Reflection symmetries:
 - (a) P_x : $\sigma_x \rightarrow \sigma_x, k_y \rightarrow -k_y, \sigma_y \rightarrow -\sigma_y, k_z \rightarrow -k_z, \sigma_z \rightarrow -\sigma_z$.
 - (b) P_y : $\sigma_y \rightarrow \sigma_y, k_x \rightarrow -k_x, \sigma_x \rightarrow -\sigma_x, k_z \rightarrow -k_z, \sigma_z \rightarrow -\sigma_z$.
 - (c) P_z : $\sigma_z \rightarrow \sigma_z, k_x \rightarrow -k_x, \sigma_x \rightarrow -\sigma_x, k_y \rightarrow -k_y, \sigma_y \rightarrow -\sigma_y$.

Note that the P_z symmetry is also equivalent to a joint π rotation of orbital and spin around \hat{z} axis. so it is not a new symmetry. The P_y can also be taken as P_x combined with $[U(1)_{spin} \times U(1)_{orbit}]_D$ by an angle $\pi/2$.

In the helicity basis Fig.M1a, pick up \vec{q} as the \hat{z} axis, then $q_x = q_y = 0, q_z > 0, \vec{q} = q_z \hat{z}$ in this helicity basis. The $[SU(2)_{spin} \times SO(3)_{orbit}]_D$ symmetry along this \hat{z} axis dictates that

$$R_z^T \chi^{\mu\nu} R_z = \chi^{\mu\nu} \quad (S1)$$

Expanding it leads to the fact that the dynamical 4×4 density-spin response function $\chi^{\mu\nu}(\vec{q}, \omega)$ can be split into two 2×2 subspaces: i) $n - L$ subspace ii) $T_1 - T_2$ subspace with $\chi^{xx} = \chi^{yy}, \chi^{xy} = -\chi^{yx}$.

(1) In the $T_1 - T_2$ subspace

After a unitary transformation, it can be shown that in the $T_1 - T_2$ subspace:

$$\chi = \begin{pmatrix} \chi^{+-} & 0 \\ 0 & \chi^{-+} \end{pmatrix} \quad (S2)$$

where $\chi^{+-} = 2(\chi^{xx} - i\chi^{xy}), \chi^{-+} = 2(\chi^{xx} + i\chi^{xy}), \chi^{++} = \chi^{--} = 0$.

The P_x (or P_y) symmetry dictates

$$\chi^{+-}(\vec{q}, \omega) = \chi^{-+}(-\vec{q}, \omega) \quad (S3)$$

The T symmetry leads to

$$\chi^{+-}(\vec{q}, \omega) = \chi^{-+}(-\vec{q}, \omega) \quad (S4)$$

which is identical to Eqn.S3.

Eqn.S3 leads to $\chi^{xx} = \chi^{yy}$ is an even function of $q_z, \chi^{xy} = -\chi^{yx}$ is an odd function of q_z .

Directly taking complex conjugate leads to:

$$[\chi^{+-}(\vec{q}, \omega)]^* = \chi^{-+}(-\vec{q}, -\omega) \quad (S5)$$

which, combining with Eqn.S3, leads to

$$\begin{aligned} \text{Re}\chi^{+-}(\vec{q}, \omega) &= \text{Re}\chi^{+-}(\vec{q}, -\omega) \\ \text{Im}\chi^{+-}(\vec{q}, \omega) &= -\text{Im}\chi^{+-}(\vec{q}, -\omega) \end{aligned} \quad (S6)$$

(a) Outside the P-H continuum, in the $T_1 - T_2$ subspace, χ^{+-}, χ^{-+} are real, so Eqn.S6 leads to the fact that $\chi^{xx} = \chi^{yy}$ and $\chi^{xy} = -\chi^{yx}$ are all even function of ω . The poles of χ^{+-}, χ^{-+} lead to the two gapped transverse modes T_{\pm} respectively.

(b) Inside the P-H, χ^{+-}, χ^{-+} have both real and imaginary parts, Eqn.S6 leads to $\text{Re}\chi^{+-}(\vec{q}, \omega)$ is an even function of ω , while $\text{Im}\chi^{+-}(\vec{q}, \omega)$ is an odd function of ω . $\text{Im}\chi^{+-}(\vec{q}, \omega) \neq 0$ leads to the particle hole excitation spectrum in the $T_1 - T_2$ subspace.

(2) In the $n - L$ subspace

The P_x (or P_y) symmetry dictates

$$\begin{aligned} \chi^{nn}(\vec{q}, \omega) &= \chi^{nn}(-\vec{q}, \omega), \chi^{LL}(\vec{q}, \omega) = \chi^{LL}(-\vec{q}, \omega) \\ \chi^{nL}(\vec{q}, \omega) &= -\chi^{nL}(-\vec{q}, \omega), \chi^{Ln}(\vec{q}, \omega) = -\chi^{Ln}(-\vec{q}, \omega) \end{aligned} \quad (S7)$$

which shows χ^{nn}, χ^{LL} are even function of q_z , while χ^{nL}, χ^{Ln} are an odd function of q_z .

The T symmetry leads to

$$\begin{aligned} \chi^{nn}(\vec{q}, \omega) &= \chi^{nn}(-\vec{q}, \omega), \chi^{LL}(\vec{q}, \omega) = \chi^{LL}(-\vec{q}, \omega) \\ \chi^{nL}(\vec{q}, \omega) &= -\chi^{Ln}(-\vec{q}, \omega), \chi^{Ln}(\vec{q}, \omega) = -\chi^{nL}(-\vec{q}, \omega) \end{aligned} \quad (S8)$$

Note that P_x and T leads to two different equations in the nL component only. Combining Eqn.S7 and Eqn.S8 leads to $\chi^{nL}(\vec{q}, \omega) = \chi^{Ln}(\vec{q}, \omega)$.

Directly taking complex conjugate leads to:

$$[\chi^{ij}(\vec{q}, \omega)]^* = \chi^{ij}(-\vec{q}, -\omega), \quad i, j = n, L \quad (S9)$$

which combining with Eqn.S7 leads to

$$\begin{aligned} \text{Re}\chi^{ii}(\vec{q}, \omega) &= \text{Re}\chi^{ii}(\vec{q}, -\omega), \quad i = n, L \\ \text{Im}\chi^{ii}(\vec{q}, \omega) &= -\text{Im}\chi^{ii}(\vec{q}, -\omega) \end{aligned} \quad (S10)$$

and

$$\begin{aligned} \text{Re}\chi^{nL}(\vec{q}, \omega) &= -\text{Re}\chi^{nL}(\vec{q}, -\omega) \\ \text{Im}\chi^{nL}(\vec{q}, \omega) &= \text{Im}\chi^{nL}(\vec{q}, -\omega) \end{aligned} \quad (S11)$$

(a) Outside the P-H continuum, $\chi^{nn}, \chi^{LL}, \chi^{nL}$ are real, Eqn.S10 leads to $\chi^{nn}(\vec{q}, \omega), \chi^{LL}(\vec{q}, \omega)$ are even function of ω . However, Eqn.S11 leads to $\chi^{nL}(\vec{q}, \omega)$ is an odd function of ω , therefore $\chi^{nL}(\vec{q}, 0) = 0$. The poles of the 2×2 matrix determinant lead to one gapless sound mode and a gapped L mode.

(b) Inside the P-H, $\chi^{nn}, \chi^{LL}, \chi^{nL}$ have both real and imaginary parts, Eqn.S10,S11 lead to $\text{Re}\chi^{ii}(\vec{q}, \omega), i = n, L$ ($\text{Re}\chi^{nL}(\vec{q}, \omega)$) is an even (odd) function of ω . While $\text{Im}\chi^{ii}(\vec{q}, \omega)$ ($\text{Im}\chi^{nL}(\vec{q}, \omega)$) is an odd (even) function of ω . $\text{Im}\chi^{nL}(\vec{q}, \omega) \neq 0$ leads to the particle hole excitation spectrum in the $n - L$ subspace.

In principle, $\text{Im}\chi^{+-}(\vec{q}, \omega) \neq 0$ need not to happen at the same time as $\text{Im}\chi^{nL}(\vec{q}, \omega) \neq 0$. However, at the RPA level Eqn.S15 used in the next section, they happen at the same time. So the P-H excitation spectrum in the (T_1, T_2) space is the same as that in (n, L) space at the RPA level. Very similarly, the P-H excitation spectrum in the density channel is the same as that in the spin channel at the RPA level used in Sec.II-B.

These exact relations can be used to simplify considerably the following analytical and numerical calculations to find the 4 collective modes considerably. Any approximations such as RPA should respect these exact relations. There must be two split transverse modes T_{\pm} (Fig.1b) in the (T_1, T_2) space. The mixing of density and longitudinal mode in the (n, L) space leads to one gapless sound mode $\omega_{\vec{q}}^s = v_s q$ and one gapped (called L) mode $\omega_L(\vec{q}) = \Delta + \alpha q^2$ (Fig.1b). The $SU(2)_{spin}$ symmetry at $\vec{q} = 0$ dictates that the three gapped modes must have the same gap Δ_s at

$q = 0$. These exact relations simplify the following analytical and numerical calculations considerably.

(3) *The symmetry reason why T_+ and T_- split*

In the following, we show that in order to guarantee the two T_+, T_- modes to be degenerate, one need to have both T symmetry and the inversion symmetry $I: \vec{q} \rightarrow -\vec{q}$. The I symmetry dictates that

$$\chi^{+-}(\vec{q}, \omega) = \chi^{+-}(-\vec{q}, \omega), \chi^{-+}(\vec{q}, \omega) = \chi^{-+}(-\vec{q}, \omega) \quad (\text{S12})$$

Combining Eqn.S4 with Eqn.S12 lead to:

$$\chi^{+-}(\vec{q}, \omega) = \chi^{-+}(\vec{q}, \omega) \quad (\text{S13})$$

Alternatively, if assuming S_x symmetry: $\sigma_x \rightarrow \sigma_x, \sigma_{y,z} \rightarrow -\sigma_{y,z}$, one also find Eqn.S13.

However, it is the SOC which breaks the Inversion symmetry, so $\chi^{+-}(\vec{q}, \omega) \neq \chi^{-+}(\vec{q}, \omega)$ for $\vec{q} \neq 0$ which leads to the splitting of the two transverse modes even in the normal phase at any $\vec{q} \neq 0$. Only at $\vec{q} = 0$, the SOC vanishes, the three modes have the same gap.

As to be shown in Sec.II-B, in the conventional 3d itinerant FM phase along \hat{z} , we still have the $U^z(1)$ spin rotation symmetry around the \hat{z} axis which still leads to Eqn.S2 for any \vec{q} . One still has inversion symmetry I which leads to Eqn.S12. Indeed, the Goldstone T_+ mode $\omega = Dq^2$ from χ^{+-} in Fig.3b satisfy this relation. However, due to the breaking of T , so the T_- mode from χ^{-+} has higher energy and also at higher momentum, can be dropped (not shown in Fig.3b).

In short, in the normal phase of SOC, it is the explicit I symmetry breaking of the SOC Hamiltonian which leads to the T_{\pm} split shown in Fig.1b. However, in the FM of conventional system to be discussed in Sec.II-B, it is the spontaneous T symmetry breaking which leads to the T_{\pm} split in Fig3b. So the two splitting mechanisms are complementary to each other.

II. COLLECTIVE MODES AND P-H EXCITATIONS FOR 3D FERMI GAS WITH AND WITHOUT SOC AT THE RPA LEVEL

In the last section, we established all the possible exact relations on the density-spin response functions from the general symmetry principle. Any analytical approximations or numerical calculations must satisfy these exact relations. In this section, we will perform a concrete calculation on all the response functions at the RPA level whose poles lead to the collective modes. We also checked that they all satisfy the exact relations.

Now we can expand Eqn.M2 $\mathcal{S}[\phi_{\mu}] = \mathcal{S}^{(0)} + \mathcal{S}^{(2)} + \dots$ in terms of ϕ_{μ} . As said in the main text, the density channel ϕ_n has a non-zero imaginary saddle point value due to the finite particle density of the fermions which could be eliminated by re-defining ϕ_n as the deviation from its saddle point value. To the second order of ϕ_{μ} , we obtain

$$\mathcal{S}^{(2)} = \frac{1}{2} \int \frac{d^3 \vec{k}}{(2\pi)^3} T \sum_n \left(\frac{1}{g} \delta^{\mu\nu} - \frac{1}{4} \bar{\chi}^{\mu\nu}(\vec{k}, i\omega_n) \right) \phi^{\mu}(\vec{k}, i\omega_n) \phi^{\nu}(-\vec{k}, -i\omega_n), \quad (\text{S14})$$

where $\bar{\chi}^{\mu\nu}$ is related to the density-spin susceptibility $\chi^{\mu\nu}(\mathbf{q}, i\omega_n) = \langle s^{\mu}(\mathbf{q}, i\omega_n) s^{\nu}(-\mathbf{q}, -i\omega_n) \rangle$ via $\bar{\chi}^{00} = -\chi^{00}$, $\bar{\chi}^{0i} = i\chi^{0i}$, $\bar{\chi}^{i0} = i\chi^{i0}$, $\bar{\chi}^{ij} = \chi^{ij}$ with $i, j, = x, y, z$. The non-interacting density-spin susceptibility is given by:

$$\chi_0^{\mu\nu}(\vec{q}, i\omega_n) = \frac{1}{V} \sum_{k, sr} F_{sr}^{\mu\nu}(k+q, k) \frac{n_F(\xi_{k+q,s}) - n_F(\xi_{k,r})}{i\omega_n - (\xi_{k+q,s} - \xi_{k,r})}, \quad (\text{S15})$$

where the $\xi_{k,s}$ is the fermion spectrum with s the helicity $\hat{p} \cdot \vec{\sigma} |ps\rangle = s |ps\rangle$, the $n_F(\xi_{k,s})$ is the Fermi distribution function, the $\xi_{k+q,s} - \xi_{k,r}$ is the particle-hole excitation energy and the overlap factor $F_{sr}^{\mu\nu}(p, q) = \langle ps | \sigma^{\mu} |qr\rangle \langle qr | \sigma^{\nu} |ps\rangle$.

In the following, we apply the the RPA formalism to calculate the collective modes in the paramagnet side with the Weyl SOC and also those in the FM side of Fermi gas without SOC. It is instructive to compare the two cases: the former has explicit inversion symmetry breaking, the latter the spontaneous Time reversal symmetry breaking. It is also shown in the main text, the FM state is always superseded by TSDW or LSDW+CDW, so never a ground state in the former system, but it maybe a ground state in the latter. It is the Weyl SOC which destroys the stability of FM and favors the formation of TSDW and LSDW+CDW to be discussed in Sec.III.

A. Collective modes in the paramagnet side with SOC: Inversion symmetry breaking

As shown in the Sect.I, the $[SU(2)_{spin} \times SO(3)_{orbit}]_D$ symmetry^{1,2} dictates that the dynamical 4×4 density-spin susceptibility Eqn.S15 can be split into two 2×2 subspaces: i) $n - L$ subspace formed by the density and the longitudinal spin mode ii) $T_1 - T_2$ subspace formed by the two transverse modes. This exact decomposition simplifies the following analytical and numerical calculations considerably.

The gapless sound mode in the $n - L$ subspace, $\omega_s = v_s q$ in Fig.1b is determined by the pole of 2×2 density-spin susceptibility: $\det(1 + \frac{q}{4} \sigma_z \chi_{nL}) = 0$ with

$$\chi_0^{nL}(\vec{q}, \omega) = \frac{m(k_1^2 + k_2^2)}{2\pi^2\kappa} \begin{pmatrix} F(y) & \beta y F(y) \\ \beta y F(y) & \frac{1}{3} + \frac{\sqrt{k_R^2 + 2m\mu}}{3k_R} \beta + y^2 F(y) \end{pmatrix}, \quad (\text{S16})$$

where $k_2 > k_1$ are the two Fermi momenta in Fig.2a, $2\kappa = k_1 + k_2$ ($k_2 - k_1$) for $\mu > 0$ ($\mu < 0$), $\beta = \frac{k_2^2 - k_1^2}{k_2^2 + k_1^2}$ and $y = \omega/v_F q$, v_F the Fermi velocity, $F(y) = 1 - y \text{arccoth} y$. It is easy to see that Eqn.S16 indeed satisfies the constraints Eqn.S10 and S11. We numerically determined the velocity v_s of this gapless sound mode at $\mu/E_R = 20$ shown in Fig.2b. This sound mode corresponds to a coupled density-longitudinal spin fluctuation.

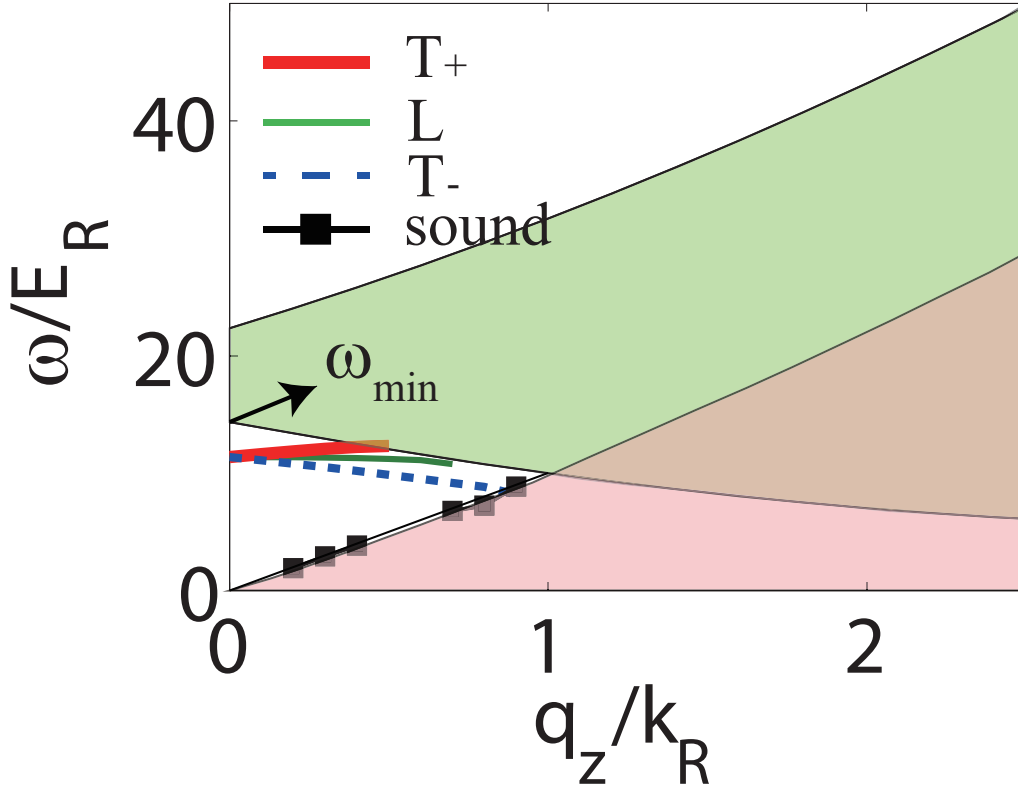


FIG. 1: (Color online) Collective modes for 3D Fermi gas with Weyl type SOC in the normal side. The parameter here are: $\mu/E_R = 20$ (equivalent to $\gamma = 0.58$) which corresponds to the case iii in Fig.2 and $a_s = 0.9a_s^c$. The green (yellow) region is the intra-band (inter-band) particle-hole excitation continuum. ω_{min} denotes the lower edge of inter-band particle-hole continuum, which is taken as the unit in Fig.2(d). In fact, (b) is re-drawing of Fig.M1b in the helicity basis. Namely, folding Fig.M1b left $q_z < 0$ back to the right $q_z > 0$ and changing the q_z axis to the q axis lead to (b). Alternatively, picking \vec{q} along the \hat{z} axis and inverting with respect to the origin gives back to Fig.M1b.

At the RPA level, from Eqn.S2, the two transverse modes are determined by

$$1 - \frac{g}{2} \chi_0^{+-}(\vec{q}, \omega) = 0, \quad 1 - \frac{g}{2} \chi_0^{-+}(\vec{q}, \omega) = 0 \quad (\text{S17})$$

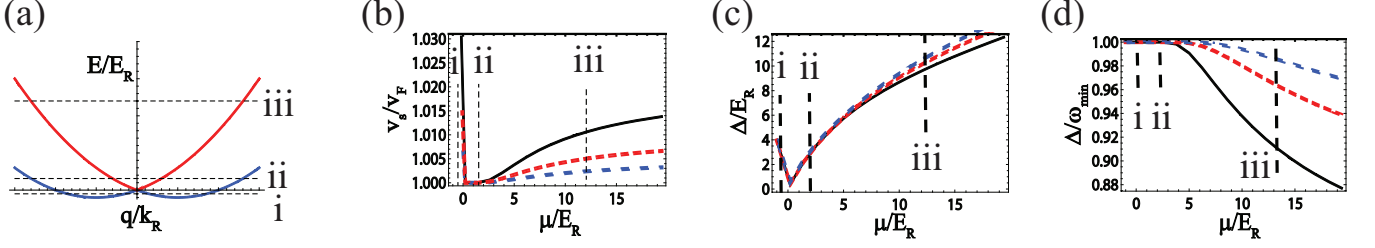


FIG. 2: (Color online) (a) Single particle energy spectrum of SOC Fermi gas in the normal state. Shown are different filling cases by the dashed lines i, ii and iii. (b) ratio v_s/v_F of gapless sound mode (c) δ/E_R and (d) δ/ω_{min} show the energy gap for the three gapped modes. The three different colors represent different interaction strengths, i.e., Black (critical interaction strength g_c for ferromagnetic phase transition), Red ($g = 4/5g_c$), Blue ($g = 2/3g_c$).

where $\chi_0^{+-}(\vec{q}, \omega) = 2(\chi^{xx} - i\chi^{xy})$ is given by Eqn.S15. Eqn.S17 lead to the T_{\pm} mode in Fig.1b.

In all, there are three branches of gapped mode, one L mode within the $n-L$ subspace and the other two T_{\pm} modes within the $T_1 - T_2$ subspace. Due to the $SU(2)_{spin}$ symmetry at $\vec{q} = 0$, the three gapped modes are degenerate at $\vec{q} = 0$ where the gap is determined by $\det[1 - \frac{q}{4}\chi_{spin}(\omega, \vec{q} = 0)] = 0$, with

$$\chi_{spin}^{ij}(\omega, \vec{q} = 0) = \frac{m}{6\pi^2 k_R} \left(k_2^2 - k_1^2 + \frac{m^2 \omega^2}{4k_R^2} \ln \left[\frac{4k_R^2 k_2^2 - m^2 \omega^2}{4k_R^2 k_1^2 - m^2 \omega^2} \right] \right) \delta^{ij}, \quad i, j = x, y, z, \quad (\text{S18})$$

The numerical result of this energy gap Δ at different μ/E_R is shown in Fig.2c (in units of the recoil energy $E_R = k_R^2/2m$) and Fig.2d (in units of the lower edge of inter-band particle-hole excitation energy ω_{min} shown in Fig.1b).

In Fig.2a, we plot three typical filling cases shown by the dashed lines: i) dilute density case with $\mu < 0$; ii) $\mu > 0$ but close to the Dirac point ($\mu = 0$), iii) dense density case. Fig.1b belongs to the case iii. In Fig.2(b), as the filling tends to the Dirac point from above $\mu > 0$, the v_s/v_F decreases close to 1. Pass the Dirac point, the ratio increases quickly. In Fig.2(c), the Δ/E_R decreases close to zero (At the Dirac point, the blank regime between the inter-band and intra-band particle-hole excitation shown in Fig.1b shrinks to zero). Pass the Dirac point, the ratio increases also. To show the relationship between the energy gap Δ and the P-H excitation, in Fig.2d we show Δ/ω_{min} with ω_{min} the lower edge of the inter-band particle-hole excitation energy shown in Fig.1b. We find as the chemical potential decreases from iii to i, the ratios gets to 1 from below, namely, the gapped collective modes move more closer to the edge of inter-band particle-hole excitation continuum in Fig.1b. In the dilute limit $\mu \rightarrow -1$, the critical interaction strength to get to FM $g_c = 12\pi^2 \sqrt{1+\mu} + \mathcal{O}((1+\mu)^{3/2})$ reduces to zero, the sound velocity saturates $v_s/v_F \simeq 1.102$, the energy gap increases and moves close to the P-H continuum $\Delta_s/E_R \simeq 4(1 - \sqrt{1+\mu})$.

The level repulsion in the $n-L$ space will push the sound mode quite close to the intra-band P-H continuum (Fig.1b,2b). Similarly, the level repulsion in the T_1, T_2 space will also split the two transverse modes T_{\pm} . So at finite, but small q , the three modes split with $\omega_{T_+} > \omega_L > \omega_{T_-}$.

B. Collective modes in the FM without SOC: Time reversal symmetry breaking:

As analyzed in Sec.I-A-2, in the normal phase of SOC, it is the I symmetry breaking in the SOC Hamiltonian which leads to the T_{\pm} split shown in Fig.1b. However, in the FM of conventional system, it is the spontaneous T symmetry breaking which leads to the split T_{\pm} in Fig3b where only T_+ is shown. So the two splitting mechanisms are complementary to each other. Here it is instructive to perform a detailed calculation on the T_{\pm} mode in the FM of conventional system. To the best of the authors knowledge, there are no previous literatures to discuss this important and tricky physical picture.

In the normal side, due to the $SU(2)_{spin} \times SO(3)_{orbit}$ symmetry, the density and spin are decoupled, the density and spin susceptibility are $\chi^{\mu\nu} = \chi_0 \delta^{\mu\nu}$ where $\mu, \nu = n, s_x, s_y, s_z$. Since the interaction is repulsive (attractive) in the density (spin) channel, there is only one gapless density mode with linear dispersion $\omega_q = v_s q$, i.e., zero sound in the density channel, no stable collective modes in the spin channel (Fig.3a).

In the FM side, there is a spin polarization \vec{M} along \hat{z} , the symmetry breaking pattern is $SU(2)_{spin} \rightarrow U(1)_z$. The

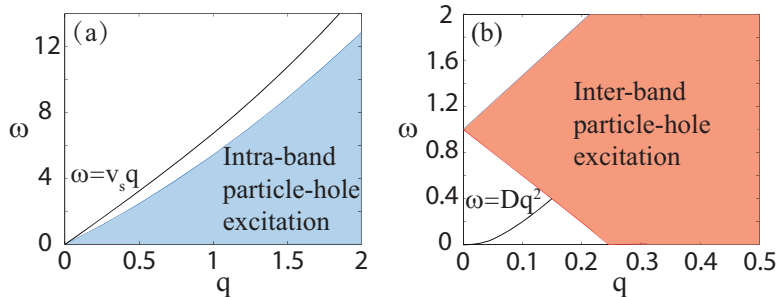


FIG. 3: (Color online) The particle-hole continuum and collective modes in traditional Fermi gas (a) zero sound in the normal side and (b) only the T_+ mode is shown in the FM side.

fermion propagator takes the form:

$$\mathcal{G}(i\omega_n, \vec{k}) = \frac{1}{2} \sum_{s=\pm 1} \frac{\sigma_0 + s\sigma_z}{i\omega_n - \vec{k}^2/2m + sgM/4}. \quad (\text{S19})$$

As said above, the remaining symmetry $U(1)_z$ dictates that the density-spin susceptibility $\chi^{\mu\nu}$, $\mu, \nu = n, s_x, s_y, s_z$ can be decoupled to two 2×2 matrixes: one for the density and longitudinal spin mode $\hat{L} = \vec{M}/M$, another for the two transverse spin modes $\hat{T}_1 \cdot \vec{M} = \hat{T}_2 \cdot \vec{M} = 0$. In the density-longitudinal subspace, the density fluctuation is strongly coupled with the longitudinal spin fluctuation, the 2×2 susceptibility takes the form:

$$\chi^{nL} = \chi_0 \begin{pmatrix} 1 & -1 \\ -1 & 1 \end{pmatrix}, \quad (\text{S20})$$

where $\chi_0 = \frac{mk_F^2}{4\pi^2} (2 + y \ln \frac{y-1}{y+1})$ with $y = m\omega/k_F q$. Due to the absence of any poles in $\det[1 + \frac{q}{4}\sigma_z \chi^{nL}] = 0$, there are no collective modes in the $n - L$ subspace.

However, in the transverse (T_1, T_2) subspace, Eqn.S2 still holds, there is only one low energy collective mode: the T_+ mode $\omega_q = Dq^2$ at small q , which couples only to the inter-band P-H excitations at higher q (Fig.3b). While the T_- mode has higher momentum and higher energy, so not shown in Fig.3b.

III. FERMI SURFACE RE-CONSTRUCTIONS IN THE PRESENCE OF SDW ORDER

A. Symmetry analysis at the BZ boundaries and the Dirac point

In the presence of T/L-SDW order, the fermionic spectrum forms energy bands. The intersection of Fermi surface will be opened due to the open of the energy bands. In the presence of SOC, there are two Fermi surfaces (FS), which leads to two kinds of FS intersection. One is that between the same FS which happens at the BZ boundary and the that at $k_z = 0$; the other type is that between the different FS, which usually happens inside the BZ boundary but $k_z \neq 0$ (exceptions could happen but are not general cases). Both analytical and numerical calculation show that: 1, the spectrum intersection at the BZ boundary will open a gap in the presence of T-SDW order but keep closed in the presence of L-SDW order; 2, the spectrum intersection at the $k = 0$ axis will keep closed in the presence of both kinds of SDW orders; as a result, the Dirac cone is kept; 3, band gap exists in general for other cases.

The above results can be illustrated by symmetry argument. First, let's summarize the remaining symmetry of the two phases with SDW orders. We find, both the T-SDW and L-SDW order are invariant up to a different corresponding translation ($T_r(a)$ with a the distance along \hat{z} direction) under the following symmetries: 1. $[SO(2)_z \times U(1)_z]_D$; 2. $\mathcal{P}_x, \mathcal{P}_y, \mathcal{P}_z$; 3. the time reversal symmetry. Besides, the translational symmetry is broken to a discrete symmetry, which leads to the band structure.

First, for T-SDW order assumed to be $\vec{\phi} = \phi(\cos Qz, -\sin Qz, 0)$, continuous rotational symmetry about z axis leads to that the spectrum is rotational symmetric about the k_z axis. Therefore, we can only consider the case with $k_y = 0$. We find the T-SDW order preserves the \mathcal{P}_x and the $\mathcal{P}'_y = \mathcal{P}_y + T_r(\frac{\pi}{Q})$ symmetry, where the prime in the subscript indicates a combined translation. The Hamiltonian is real and therefore, all of its eigenstates can

be chosen to be real vectors. To consider the single particle eigen-states with given momentum \vec{k} in the first BZ, the \mathcal{P}_x (\mathcal{P}'_y) symmetry operating on these eigen-states will be closed only at places where $k_z = -Q/2$, i.e., the BZ boundary, or $k_z = 0$ ($(k_x, k_z) = (0, -Q/2)$ or $\vec{k} = 0$). We first apply the \mathcal{P}_x symmetry. Due to the periodic SDW order, the ground state is a superposition of the states $|\vec{k}, n, \sigma\rangle$, where the momentum is given by $\vec{k} + nQ\hat{e}_z$ with $n = 0, \pm 1, \pm 2, \dots$, $\sigma = 1, 2$ which represents spin \uparrow and \downarrow . The \mathcal{P}_x symmetry gives rise to the following transformation: $|(k_x, 0, k_z), n, \sigma\rangle \rightarrow |(k_x, 0, -k_z), -n, \bar{\sigma}\rangle$ with $\bar{\sigma}$ represents the opposite spin component with respect to σ . We assume the eigen-wave function at the BZ boundary to be:

$$|\Psi\rangle_{BZ} = \sum_{n;\sigma} a_{n\sigma} \left| \frac{2n+1}{2}Q, \sigma \right\rangle, \quad (\text{S21})$$

where $\frac{2n+1}{2}Q$ represents the k_z component of \vec{k} . Here and after, we will ignore the k_x component unless it is specialized. Since the Hamiltonian is real, the coefficients $a_{n\sigma}$ can be chosen to be real values. The \mathcal{P}_x symmetry leads to

$$\mathcal{P}_x |\Psi\rangle_{BZ} = \sum_{n;\sigma} a_{n\sigma} \left| -\frac{2n+1}{2}Q, \bar{\sigma} \right\rangle. \quad (\text{S22})$$

Applying this operation twice, we find $\mathcal{P}_x^2 |\Psi\rangle_{BZ} = |\Psi\rangle_{BZ}$. At $\vec{k} = 0$, the wavefunction is assumed to be

$$|\Psi\rangle_0 = \sum_{n;\sigma} a_{n\sigma} |nQ, \sigma\rangle. \quad (\text{S23})$$

The \mathcal{P}_x symmetry acting this wavefunction twice also leads to $\mathcal{P}_x^2 |\Psi\rangle_0 = |\Psi\rangle_0$. This symmetry is not sufficient to guarantee the two-fold degeneracy at the BZ boundary and $\vec{k} = 0$. Then, we apply the \mathcal{P}'_y symmetry at $\vec{k} = 0$, which gives rise to

$$\mathcal{P}'_y |\Psi\rangle_0 = \sum_{n;\sigma} (-1)^n (-1)^\sigma a_{n\sigma} | -nQ, \bar{\sigma} \rangle. \quad (\text{S24})$$

Applying this operation twice, we find $\mathcal{P}'_y{}^2 |\Psi\rangle_0 = -|\Psi\rangle_0$. Due to this property combined with the fact that the Hamiltonian is real, the energy spectrum at $\vec{k} = 0$ will have a two-fold degeneracy. The Dirac cone structure is preserved in the presence of T-SDW order. If we apply the \mathcal{P}'_y symmetry at $(k_x, k_z) = (0, -Q/2)$, there will be $\mathcal{P}'_y{}^2 |\Psi\rangle_{BZ} = |\Psi\rangle_{BZ}$, which fails to preserve the two-fold degeneracy.

We can similarly consider the LSDW order. The order parameter assumed as $\vec{\phi} = \phi(0, 0, \cos Qz)$ is invariant under both the $\mathcal{P}'_x = \mathcal{P}_x + T_r(\frac{\pi}{Q})$ and $\mathcal{P}'_y = \mathcal{P}_y + T_r(\frac{\pi}{Q})$ symmetry. The Hamiltonian is real and therefore, all of its eigenstates can be chosen to be real vectors. At the BZ boundary, the form of the wavefunction is given by Eq. (S21). Then, we apply the \mathcal{P}'_x symmetry and find that

$$\mathcal{P}'_x |\Psi\rangle_{BZ} = \sum_{n;\sigma} (-1)^n a_{n\sigma} \left| -\frac{2n+1}{2}Q, \bar{\sigma} \right\rangle. \quad (\text{S25})$$

Applying \mathcal{P}'_x symmetry twice, we obtain $\mathcal{P}'_x{}^2 |\Psi\rangle_{BZ} = -|\Psi\rangle_{BZ}$. Due to this property combined with the fact that the Hamiltonian is real, the energy spectrum at the BZ boundary has a two-fold degeneracy. Then, we consider the situation at $\vec{k} = 0$. The \mathcal{P}'_x symmetry would leads to $\mathcal{P}'_x{}^2 |\Psi\rangle_0 = |\Psi\rangle_0$ which is not sufficient to guarantee the two-fold degeneration. We consider again the \mathcal{P}'_y symmetry, which is the same as the situation we have encountered in the case of T-SDW order. Therefore, it guarantees the two-fold degeneracy at $\vec{k} = 0$ but not sufficient at $(k_x, k_z) = (0, -Q/2)$. The Dirac cone structure is also preserved in the presence of L-SDW order.

As we have shown in the main text, the LSDW would induce a CDW order with orbital momentum $2Q$. Because the density order is invariant under the above symmetry operations, all of these results would not change. Any other places of the BZ would not be preserved by symmetry properties, therefore, there is a band gap opening when the T/L-SDW order is eigenegered.

B. Two-level degenerate perturbations

Due to the periodic order, the list of states $|k + nQ, \pm\rangle$ are coupled together. If two of the list of states are degenerate, there will be a level intersection there.

(1) At the BZ boundaries

This always happens at the BZ boundary, where a list of states $|(n - \frac{1}{2})Q, \pm\rangle$ are coupled together. One can find $|(n + \frac{1}{2})Q, s\rangle$ and $|-(n + \frac{1}{2})Q, s\rangle$ forms a degenerate pair. As an example, we can consider the lowest band with $n = 0$ and $s = -1$. For T-SDW order, the two by two Hamiltonian is given by:

$$\mathcal{H}_{T-SDW} = \begin{pmatrix} \mu & -\frac{\phi}{2} \sin^2 \frac{\theta}{2} e^{-i\varphi} \\ -\frac{\phi}{2} \sin^2 \frac{\theta}{2} e^{i\varphi} & \mu \end{pmatrix}, \quad (\text{S26})$$

where $\mu = \xi_{Q/2,-}$, θ, φ is the azimuthal angle of $k = (k_x, 0, Q/2)$ with $\theta < \pi/2$. The resulting spectrum is given by

$$\xi_s = \xi_{Q/2,-} + s \frac{\phi}{2} \sin^2 \frac{\theta}{2}, \quad (\text{S27})$$

and the band gap is naturally given by $\Delta = \phi \sin^2 \frac{\theta}{2}, \theta < \pi/2$. Similarly for $k = (k_x, 0, -Q/2)$ with $\theta > \pi/2$, we obtain the band gap as $\Delta = \phi \cos^2 \frac{\theta}{2}, \theta > \pi/2$. By contrast, for L-SDW order, one can find the coupling term between $|(n + \frac{1}{2})Q, s\rangle$ and $|-(n + \frac{1}{2})Q, s\rangle$ is always zero. So, there is no band gap opening to this order, which is consistent with the above Exact symmetry analysis valid to any order of perturbations.

(2) At the intersections between the large and small FS inside the BZ

Since there are two energy branches due to SOC, there will be intersection between them, where the states $|k + nQ, s\rangle$ and $|k + mQ, r\rangle$ are coupled together. If m and n are different by one, we can apply a simple two-level degenerate perturbative calculation, where the Hamiltonian is given by

$$\mathcal{H}_{T/L-SDW} = \begin{pmatrix} \mu & \phi M \\ \phi M^* & \mu \end{pmatrix}, \quad (\text{S28})$$

where μ is the degenerate energy level, $M = \frac{1}{2}\langle k_1, s | \sigma^+ | k_2, r \rangle$ for T-SDW order while $M = \frac{1}{4}\langle k_1, s | \sigma^z | k_2, r \rangle$ for L-SDW order. There will be a band gap given by $\Delta = 2\phi|M|$.

We assume $s = -r = 1$ corresponding to intersection between different helicity branches, which could happen in high energy regime. For T-SDW order, there is $M = -\frac{1}{2} \cos \frac{\theta_1}{2} \cos \frac{\theta_2}{2} e^{i\varphi_2}$, where $\theta_{1,2}, \varphi_1 = \varphi_2$ are the azimuthal angles of $k_{1,2}$. While for L-SDW order, there is $M = \frac{1}{4}(\cos \frac{\theta_1}{2} \sin \frac{\theta_2}{2} - \sin \frac{\theta_1}{2} \cos \frac{\theta_2}{2}) = -\frac{1}{4} \sin \frac{(\theta_1 - \theta_2)}{2}$.

Similarly, we can also consider $s = r = -1$ corresponding to intersection between the minus helicity branches, which could happen at low energy regime. For T-SDW order, $M = -\frac{1}{2} \sin \frac{\theta_1}{2} \cos \frac{\theta_2}{2} e^{i\varphi_2}$; for L-SDW order, $M = \frac{1}{4}(\sin \frac{\theta_1}{2} \sin \frac{\theta_2}{2} - \cos \frac{\theta_1}{2} \cos \frac{\theta_2}{2}) = -\frac{1}{4} \cos \frac{(\theta_1 + \theta_2)}{2}$.

¹ For the exact constraints on the pairing length from the spin-orbit coupled symmetries, see Yi-Xiang Yu, Jinwu Ye, Wu-Ming Liu, Phys. Rev. A 90, 053603 (2014).

² For the exact constraints on the correlation functions on a lattice from the spin-orbit coupled symmetries, see Fadi Sun, Jinwu Ye, Wu-Ming Liu, arXiv:1408.3399.